Design of metal@titanium oxide nano-heterodimers by laser-driven photodeposition: growth mechanism and modeling

Qingguo Bai, Ivan Shupyk, Laetitia Vauriot, Jérôme Majimel, Christine Labrugère, Marie-Hélène Delville, Jean-Pierre Delville

Design of Metal@Titanium Oxide Nano-Heterodimers by Laser-Driven Photodeposition: Growth Mechanism and Modeling

Qingguo Bai[1,2], Ivan Shupyk[1,2], Laetitia Vauriot[1,2], Jerome Majimel[1], Christine Labrugere[3], Marie-Helene Delville[1], and Jean-Pierre Delville[2*]*

[1] CNRS, Univ. Bordeaux, Bordeaux INP, ICMCB, UMR 5026, 87 avenue du Dr. A. Schweitzer, Pessac, F-33608, France.

[2] Univ. Bordeaux, CNRS, LOMA, UMR 5798, 33405 Talence, France.

[3] CNRS, Univ. Bordeaux, PLACAMAT, UMS 3626, 87 avenue du Dr. A. Schweitzer, Pessac, F-33608, France.

ABSTRACT: In order to circumvent the usual nucleation of randomly distributed tiny metallic dots photodeposited on TiO_2 nanoparticles (NPs) induced by conventional UV lamps, we propose to synthesize well-controlled nanoheterodimers (NHDs) using lasers focused inside microfluidic reactors to strongly photoactivate redox reactions of active ions flowing along with nanoparticles in water solution. Since the flux of photons issued from a focused laser may be orders of magnitude higher than that reachable with classical lamps, the

production of electron-hole pairs is tremendously increased, ensuring a large availability of carriers for the deposition and favoring the growth of a single metallic dot as compared to secondary nucleation events. We show that the growth of single silver or gold nanodots can be controlled by varying the beam intensity, the concentration of the metallic salt, and the flow velocity inside the micro-reactor. The confrontation to a build-in model of the metallic nanodot light-induced growth onto the surface of TiO_2 NPs shows the emergence of a predictable 'master behavior' on which individual growths obtained from various tested conditions do collapse. We also characterized the associated quantum yield. Eventually, we successfully confronted our model to growth data from the literature in the case of silver on TiO_2 and gold on II-VI semiconducting NPs triggered by UV lamps. It shows that for the photosynthesis of NHDs, the efficiency of the electron-hole pairs production rate matters much more than the number of pairs produced and that the use of laser light can provide a photodeposition-based synthesis at the nanoscale.

Keywords: photodeposition, laser, nano-heterodimers, optofluidic, TiO_2, silver, gold

INTRODUCTION

The discovery of platinum photo-loading on TiO_2 nanoparticles (NPs) by Kraeutler and Bard in 1978[1] has triggered a tremendous interest in the photochemical deposition of metals on semiconductor substrates for the last forty years. It led to extensive applications in various domains as different as photocatalysis,[2] solar cells,[3] water treatment[4] and splitting, [5]metal recovery,[6] photo-imaging,[7] and many other areas[8] to cite a few of them. Photodeposition is indeed very attractive since it does not need any complex dedicated setups. It only requires the light exposure, at an optical wavelength within the band gap of the considered semiconductor to produce electron-hole pairs, of a solution containing the semiconductor NPs, the metallic ions to be reduced and a hole scavenger to be oxidized, with some compatible conditions regarding reduction/oxidation potentials of both metal and semiconductor. This versatility, combined with the increasing importance of photocatalysis for 'green chemistry', explains why this simple optical excitation technique has been so largely employed to synthesize so-called metal-loaded NPs with so many semiconductor substrates and metals, offering a large panel of possibilities for dedicated applications.[9]

However, as mentioned in the perspectives of a recent extensive review,[10] the optimization of the photodeposition processes often remains empirical due to the actual limitations in our understanding between the core/interface properties of photo-excited NPs and the heterogeneous photo-nucleation mechanisms. Therefore, even if the photodeposition may allow some reproducibility of the size of the deposited metal dots and of their statistical distribution over the substrate,[11] it leads to a poor control on their number. As far as we know, we are aware of three exceptions to this well-documented general trend. The first one seems to be specific to II-VI semiconductor substrates such as CdS and CdSe/CdS quantum rods.[12-13] In this case, the photodeposition may nicely and robustly end up with the formation of nanoheterodimers (NHDs) with a single gold nanodot (ND) deposited on one of the tips of the

rods; the size of this gold ND can as well be well- controlled.[14] The two other exceptions are related to common metal oxide semiconductors on which photodeposition generally almost systematically produces a randomly distributed assembly of tiny metallic NDs.[15-16] In one of them, the silver photodeposition on TiO_2 nanorods revealed that numerous dots were photo-nucleated, as expected, but then progressively dissolved and eventually ripened into a single large ND under prolonged UV exposure.[17] The second experiment involves the photodeposition of a single silver ND on ZnO nanorods[18] but it seems quite isolated when compared to the further well-documented works published on metal deposition onto ZnO.[19-21]

The nucleation and growth of a single metallic dot are indeed of major significance when considering recent experiments on photocatalysis efficiency where it has been clearly shown for certain reactions, that a single metallic ND is much more efficient than several ones,[22] and that the control and the adjustment of the size of this ND is also crucial to increase the yields.[23-25] However, up to now, such a versatile control using photodeposition remains limited to some II-VI semi-conductors and the photodeposition on more common and less toxic metal oxides does not seem to be able to reach these requirements in size and number of photodeposits.

With TiO_2 anatase NPs on the one hand and silver and gold precursors on the other one, we experimentally show in this work how this photodeposition 'glass ceiling' can be broken. For this purpose, we use focused laser beams, instead of UV lamps to proceed to the generation of effective metal oxide-based NHDs in a microchannel configuration. Since the photons flux density from a focused laser can be made orders of magnitude higher than that issued from a spectral lamp, the electron-hole pair production is tremendously increased so that the electron availability for the metal deposition is not any more sensitive to the trapping by the bulk or the surface defects of the semiconducting NPs. Consequently, when a first deposit is nucleated, a very high electric field gradient is produced inside the TiO_2 NPs that strongly

favors the metal ND growth,[26] as compared to secondary nucleation events elsewhere at the surface of TiO_2. Once formed, this ND enhances in return electron-hole pair separations as opposed to recombination, the two effects promoting the formation of NHDs.[27] We experimentally demonstrate this property of laser-deposition and show that the deposit growth and size, are both controlled by the injected beam intensity (for the electron-hole pair production), by the flow rate of the NPs solution (for the time exposure involved for this production), and by the metal ion concentration in the solution (for the amount of photo-deposable material). Moreover, we developed a general model that quantitatively describes the growth of metallic NDs onto semiconducting NPs, thus providing a general scheme for the synthesis of semiconductor/metal NHDs and a predictive approach for their growth in different conditions. Finally, the flow of the solution inside a channel ensures a continuous production of NHDs.

RESULTS AND DISCUSSION

Setup & Methodology

The principle of our laser-deposition setup is illustrated in Figure 1 (a detailed description of the setup is given in Supporting Information S1). A water solution containing TiO_2 anatase as semiconducting NPs (mean size (25 ± 4) x (25 ± 4) x (40 ± 6) nm^3, 5.5 mM, Supporting Information S2 for their full characterization), silver nitrate (2 mM) as a metallic precursor and methanol (50% v/v) as hole scavenger, is flowing through a microchannel and crossing an exciting laser beam. The pH of the solution is adjusted to 3.5 with 0.1 M HNO_3 to preserve the colloidal stability of the TiO_2 NPs. These TiO_2 anatase NPs were synthesized using a temperature hydrothermal procedure without any follow-up heat treatment according to a literature procedure[28] to make sure the initial particles were well-individualized ones (see Material section and Supporting Information Figure S2) and to prevent sintering as observed in the case of P25.

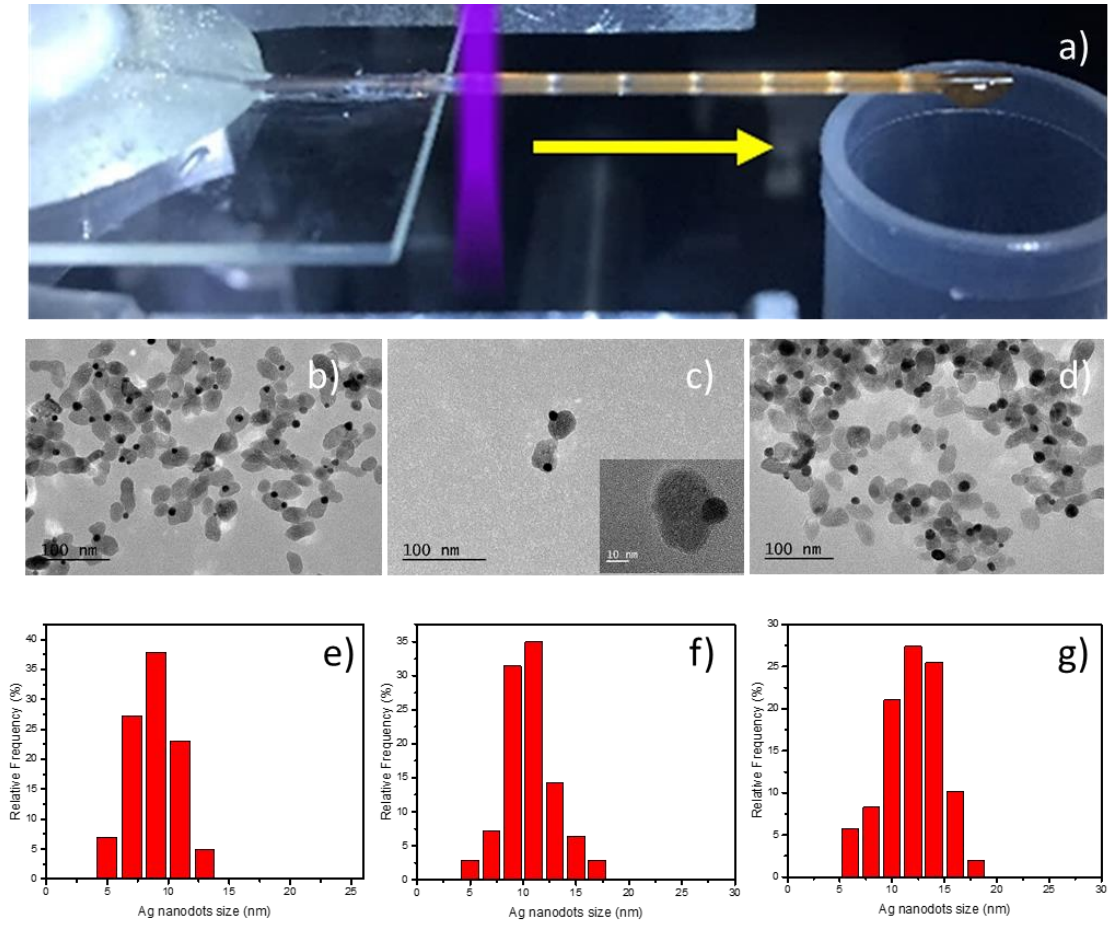

Figure 1. a) Picture of the experimental set-up used for the photo-production of the (NHDs) TiO_2/M in a microchannel configuration (M = Ag in this case); note the color change of the solution from transparent to brownish after crossing the laser beam (the solution flows from left to right according to the direction of the yellow arrow). TEM images of NHDs obtained by laser-deposition at a mean flow velocity v = 960 µm/s and beam intensities of b) I = 16.4, c) I = 24.6 (a low NHDs concentration region is displayed here to focus on the one to one nature of the NHDs) and d) I = 82.0 W/cm^2, with the corresponding size distributions e), f), g). TiO_2 anatase NPs (5.5 mM), silver nitrate (2 mM), and methanol (12.34 M), pH 3.5.

The solution is infused in a homemade glass microchannel using syringe pumps (KD Scientific) *via* two possible ways. (i) The solution simply flows in a single square glass channel of internal size 600 µm (from Vitrocom™). (ii) The solution flows concomitantly with a long chain alkane solvent (here at a volume ratio *n*-dodecane/NPs solution of 20%) in a

home-made chip composed of two glass channels, a round one (of external diameter 550 μm) for the NPs solution, partially inserted in the square one (of internal size 600 μm), now used for the oil injection (see Supporting Information S3 and Figures S3 a and b); the final co-flow in the square channel is exposed to the local laser excitation, as illustrated in Figure 1a. The square channel is silanized to increase the wall wettability of the flowing alkane. Due to interfacial tension, the two-phase flow consists in long drops of aqueous solutions surrounded by *n*-dodecane as illustrated in Figure 1a (see also Movie 1 in Supporting Information). The advantage of using two-phase flows is the generation of a thin dielectric organic layer, here composed of *n*-dodecane, between the channel walls and the long aqueous drops of the NPs solution that hardly wets the internal glass surface and surely prevents any possible photoactivation of trapped charges on the glass walls. A non-ionic surfactant (sorbitan monooleate Span 80,[29] 15 mM) can be added to the alkane in order to increase even more its wettability on the channel walls. Moreover, the mean flow velocity inside the square channel, required to determine the exposure time to the laser of the flowing NPs, is varied with the syringe pumps while keeping a constant 4:1 aqueous-alkane solution flow rate ratio, and determined by following the interfaces of the flowing solution drops using a CCD video camera. When single channels are used, the mean flow velocity is simply determined from the imposed flow rate and the channel section. In Figure 1 for example, the imposed droplet velocity is v = 960 μm/s.

Since the band gap of TiO_2 anatase is Eg ~ 3.2 eV, we implemented the photo-excitation of the aqueous solution using a continuous Ar^+ laser (Innova 305C, Coherent) working in UV at λ_0 = 363.8 nm in vacuum. This wavelength was chosen not too far in UV into the TiO_2 band gap so that the optical absorption of TiO_2 is already significant (see Supporting Information S4) and those of the metallic salt precursors chosen for the deposition, potassium gold tetrachloride in particular since silver nitrate is almost transparent at the chosen wavelength, are reduced as

much as possible. The laser beam is focused inside the square part of the microchannel using three lenses to properly fill transversally the 600 µm channel width, and the beam section is eventually made elliptical using a cylindrical lens to produce a 'bar of light' inside the channel and increase even more the photon flux density in the direction of the flow; the beam waists perpendicular and along the flow inside the microchannel are respectively $\omega_{0,x}$ = 215 µm and $\omega_{0,y}$ = 95 µm. Finally, the optical transmission of the whole setup is measured in order to know exactly the beam power inside the square microchannel and deduce precisely the exciting beam intensity; the setup and calibration procedures, all crucial for a quantitative modeling of the deposit growth, are presented in Supporting Information S1. Figure 1a illustrates this setup at work when a NPs solution containing silver nitrate is exposed to the UV laser at the location underlined in purple; a strong color change of the flowing solution from transparent to brownish is clearly evidenced after crossing the laser beam and already suggests the silver deposition on TiO_2 NPs. The droplets are eventually collected into a glass vial (see Figure 1a, right) in which the two phases remain separated, the orange-brown TiO_2/Ag NHDs staying in the aqueous one. The addition of a non-ionic surfactant in the alkane phase can provide an additional practical advantage. Indeed, a gentle shaking of the vial containing the two fluids after laser-deposition induces a transfer of the NHDs to the oil phase leaving a colorless aqueous phase, and thus performing a sort of self-cleaning of the reaction product that can further be diluted in shorter alkanes for analyses and uses.

TiO_2/M synthesis & Characterizations

The central beam intensity at focus inside the channel is given by $I = 2P/(\pi\, \omega_{0,x}.\omega_{0,y})$. Assuming a beam power up to P = 100 mW, the photon flux density can be as large as I = 312 W/cm^2 which allows values up to 10^4 larger than those classically used with UV lamps, typically no more than a few tens of effective mW/cm^2. Such a huge amount of photons per unit surface produces a tremendously large number of electron-hole pairs and thus rapidly

triggers the nucleation of a first silver ND on a low heterogeneous nucleation barrier defect of the TiO_2 NPs. Since intrinsically the growth is favored thermodynamically as compared to a secondary heterogeneous nucleation event on the one hand, and the presence of a metallic dot triggers a high electric field gradient in the NP on the other hand, the charge separation is then increasingly enhanced and the growth of the first nucleus is even more privileged. Note that the short exposure time, $t_{exp} = 2\omega_{0,y}/v = 0.20$ s in the conditions of Figure 1, strongly suggests the importance of the used beam intensity I as opposed to the often accepted idea that what matters is the energy deposited during the exposure time $I.t_{exp}$ (see Supporting Information S5 for a detailed comparison of photodeposition when using UV lamp and laser setups at same deposited energies). Indeed, the deposited energy per unit surface, 24 J/cm^2 in the conditions of Figure 1d, is typically equivalent to that of a UV lamp of intensity 10 mW/cm^2 used during 40 min, and nonetheless the photodeposition results are totally at variance; we obtain single large metallic NDs (Figure 1b-d) instead of the generation of a set of tiny dots as observed in the literature (see as well Supporting Information S5).[10] Figures 1b-d indeed show TEM images of NHDs that were obtained by such a laser-deposition at a mean flow velocity v = 960 µm/s and for beam intensities I = 16.4 W/cm^2 (P = 5.5 mW), I = 24.6 W/cm^2 (P = 8.0 mW) and I = 82.0 W/cm^2 (P = 26.3 mW), with the corresponding size distributions of the grown silver NDs (Figures 1e-g), measured systematically on at least 200-250 NHDs. The average size of the laser-deposited metallic NDs increases with the injected beam intensity when all other variables (metallic precursor concentration and exposure time) remain constant, and the distributions show a stable polydispersity around 20% (in the present case: 21, 23 and 22 % respectively for dots of 8.8 ± 1.9 nm, 10.6 ± 2.4 nm, 11.9 ± 2.6 nm). Finally, the measured NHDs yields are 85, 88 and 90%, respectively. Note that possible laser heating side effects, not observed in the experiments, can be confidently discarded since the

absorption of theTiO_2 NPs solution at the chosen concentration leads to a laser overheating of only 0.02 K/mW (see Supporting Information S6).

The presence of silver in the NHDs is further established by Energy Dispersive X-Ray spectroscopy (EDS) with the presence of both titanium and silver in the spectrum (Supporting Information S7, Figure S7) and comparison of their X-ray photoelectron spectroscopy (XPS) analysis (Figure 2) with that of pure TiO_2 to check the chemical oxidation state of both Ti and Ag. A close look at the high-resolution spectra (Figure 2, Supporting Information S8 & Figure S8, Table 1) shows that the Ti2p1/2 and Ti2p3/2 spin-orbit peak splitting pattern for both samples, TiO_2/Ag and TiO_2, is about 5.6-5.7 eV which is consistent with the binding energy separation observed for Ti^{4+} in stoichiometric TiO_2.[30-36] Moreover, no trace of Ti^{3+} nor of Ti^{2+} was found, for which $Ti2p_{3/2}$ locates at 457.6 (± 0.2 eV) and 456.4 (± 0.2 eV), respectively.

Table 1. Ti2p, O1s, Ag3d binding energy Assignments for TiO_2 NPs and TiO_2/Ag NHDs.

Sample	Element	Peak BE (± 0.2 eV)	FWHM (eV)
TiO_2 NPs	Ti2p3/2	458.3	1.0
	Ti2p1/2	463.9	1.94
	O1s	529.5	1.18
	O1s	531.3	1.65
TiO_2/Ag NHDs	5/2	368.6	1.0
	Ag3d3/2	374.6	1.0
	Ti2p3/2	459.1	1.2
	Ti2p1/2	464.8	2.3
	O1s	530.3	1.2
	O1s	531.3	1.4
	O1s	532.4	1.5
	O1s	533.5	1.5

The O1s signal of pure TiO_2 can be fitted with two Gaussian components, a main one at 529.5 (± 0.2 eV) and a shoulder located toward higher binding energies at 531.3 (± 0.2 eV). They are respectively assigned to oxygen bound to Ti^{4+} ions in TiO_2 for 529.5 (± 0.2 eV), while binding energy located at 531.6 (± 0.2 eV) can be attributed to O−H bonds of the

hydroxyl groups.[31, 36] The wide contribution at 531.3 (± 0.2 eV) is assigned to the oxygen involved in O−C and C=O bonds and related to the pollution and the carbon of the TEM grids. Indeed, the fitting of the C1s peak resulted in four peaks. Beside the main contribution at 284.6 (± 0.2 eV) of Csp2, the other peaks are attributed to oxidized forms of carbon, which are usually detected 286.2 (± 0.2 eV) (C–O); 287.8 (± 0.2 eV) (C=O, O–C–O) and 288.6 eV (COO), and were also found here (not shown).[37]

The high-resolution XPS spectra of the NHDs are illustrated in Figure 2a-b for Ti and Ag. By comparison to pure anatase TiO_2, the two peaks of Ti2p shift to higher binding energies at 459.1 and 464.7 (± 0.2 eV).[38] This shift is known and has been attributed to the interaction between Ag and TiO_2, which results in a lower electron density on the TiO_2 surface once the silver NDs are deposited.[38-39]

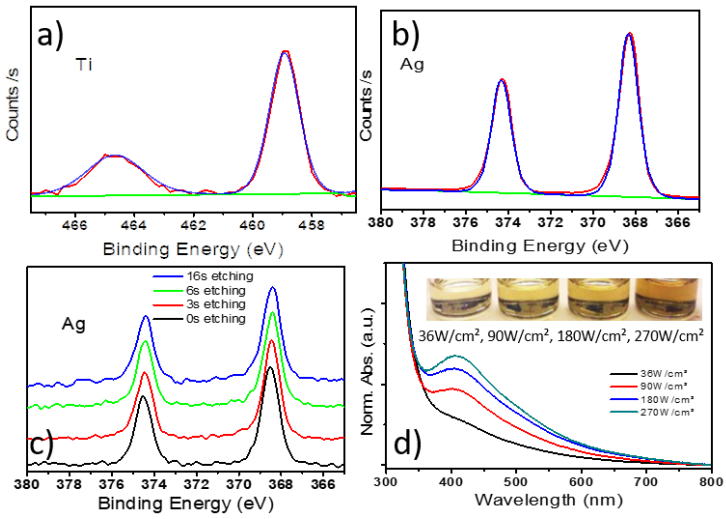

Figure 2. High-resolution XPS spectra of a) Ti2p and b) Ag3d of TiO_2/Ag NHDs; and c) variation of Ag3d through different Ar^+ etching times; d) UV-Vis spectra of the NHDs obtained by laser-deposition at a mean flow velocity v = 960 µm/s and beam intensities I = 36, 90, 180 and 270 W/cm^2 after transfer to the oil phase and dispersion in heptane. Inset: corresponding color change of the NHDs solution in heptane after identical purification treatment. TiO_2 anatase NPs (5.5 mM), silver nitrate (2 mM), methanol (12.34 M), and pH 3.5.

XPS analysis of silver element shows that this element is different from the other ones.[35, 40] Indeed, Ag is one of the rare element for which the peak position of its oxidized form Ag(I) in Ag_2O powder is shifted to lower binding energy (BE) than that of its totally reduced one Ag(0), with a value of 367.7 (± 0.2 eV). This negative BE shift is opposed to the classical positive core level BE shifts from neutral to metal cations generally found in ionic materials.[32, 34] In our case, the high resolution Ag3d XPS spectrum (Figure 2) shows the two well defined peaks at 368.6 (± 0.2 eV) and 374.6 (± 0.2 eV), assigned to the $Ag3d_{5/2}$ and $Ag3d_{3/2}$ contributions, respectively. These peaks are slightly shifted to higher BE as compared to bulk metallic Ag (368.3 (± 0.2 eV) for $Ag3d_{5/2}$, and 374.3 (± 0.2 eV) for $Ag3d_{3/2}$). This small shift can be explained by the electron transfer from the TiO_2 NP to the Ag ND.[38] These results confirm the absence of any oxidized species of silver. In the same way, the high-resolution O1s XPS spectra does not show the 528.4 (± 0.2 eV) contribution due to Ag_2O silver oxide. The observed peaks located at 531.3 (± 0.2 eV), 532.4 (± 0.2 eV) and 533.5 (± 0.2 eV) respectively correspond to the oxidized carbons (C=O and C-O) of the contamination.[37]

The UV-Vis absorption spectra of the NHDs solutions obtained after exposure at different intensities and further identical dilution in heptane (Figure 2d) show as well, beyond the expected extinction signal of TiO_2 NPs, the presence of another band with a maximum peak located around 410 nm of increasing amplitude with the beam intensity. This peak corresponds to the surface plasmon resonance of the silver NDs slightly shifted by the scattering component of the extinction; the width of the band is likely related to the 20% polydispersity.

The interface between the metal and TiO_2 in these NHDs produced by laser-deposition reveals to be very stable with regard to the centrifugation rate used for their purification (as high as 10,000 rpm for 30 min.). No free silver NDs were detected on TEM grids after such treatments.

They are also stable in the reaction solution under an aging process in the dark without any purification treatment up to three months as illustrated in Figure S9, which shows the stability in the case of 13 nm-size silver NDs laser-deposited on TiO_2 NPs, with an average size increase of only 2 nm in three months.

The same type of laser-deposition was performed to obtain NHDs with gold NDs. One single gold ND is evenly generated per TiO_2 NP as exemplified in Figure 3 for TiO_2 anatase NPs (5.5 mM), potassium gold tetrachloride (2 mM), and methanol (12.34 M), at pH 3.5. The yields in TiO_2/Au NHDs are lower than those for TiO_2/Ag, (around 50% as compared to the 90% yield for silver ND deposition), likely due to the fact that three electrons are required to produce a gold atom which is statistically much less favorable than the single electron process needed to reduce a silver ion. This figure gathers the TEM image of such NHDs obtained by laser-deposition at a mean flow velocity v = 960 µm/s and beam intensity I = 72.5 W/cm^2 (Figure 3a) and their size distribution (Figure 3b). Their UV-Vis spectrum reveals the emergence of the surface plasmon resonance around 550 nm expected for a solution of gold NDs and illustrated in the Inset by the purple color of the solution after laser-deposition. The XPS High-resolution spectra of Au4f with peaks at binding energies 87.7 eV (± 0.2 eV) (Au4f5/2) and 84.0 eV (± 0.2 eV) (Au4f7/2) (Figure 3e)[41] show that gold is in its metallic form and no Au bonded to oxygen with binding energies 85.8 (± 0.2 eV) and 89.5 (± 0.2 eV) eV was detected.[42]

Once again a study under different etching times was performed and no change in the metallic Au4f spectrum was detected (Figure 3f). The characteristic spectra of Ti2p, again show peaks of Ti2p3/2 and Ti2p1/2 observed at 459.4 eV (± 0.2 eV) and 465.2 eV (± 0.2 eV), respectively corresponding to Ti(IV) in TiO_2 (Figure 3d).

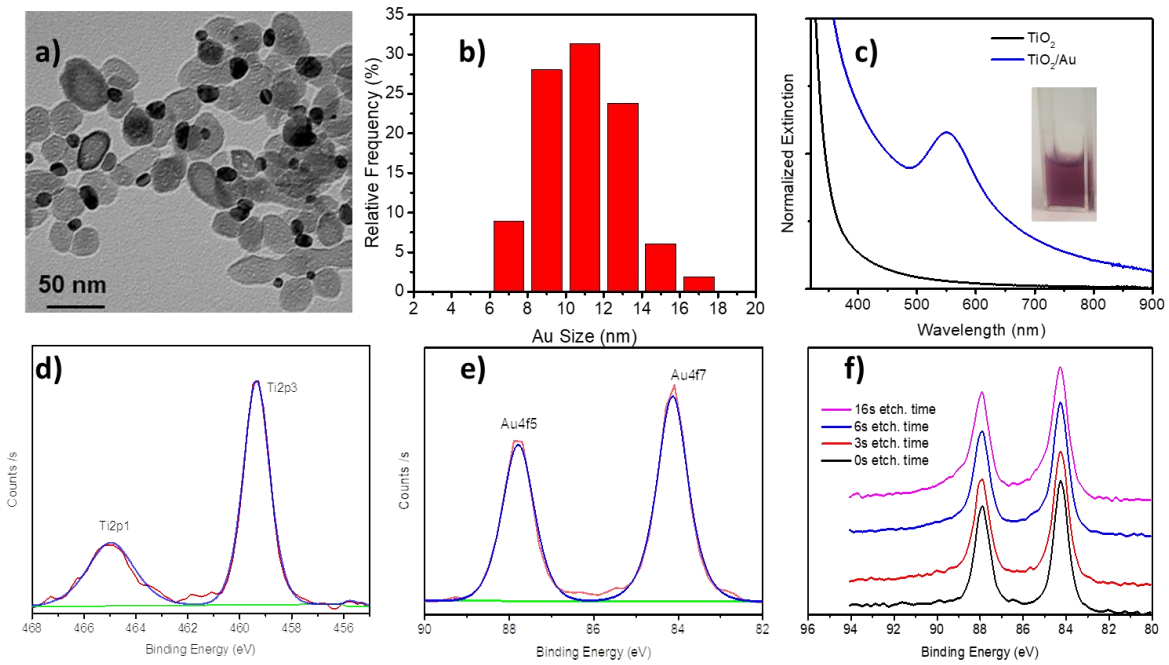

Figure 3. a) TEM image of the NHDs TiO_2/Au and b) their size distribution based on the measurement of at least 250 NHDs; c) UV-Vis spectrum in water of the same NHDs; d) and e) XPS High-resolution spectra of Ti2p and Au4f respectively; f) variation of the Au4f through different etching times. NHDs in (a) were obtained by laser-deposition at a flow velocity v = 960 µm/s and for a beam intensity I = 72.5 W/cm^2; TiO_2 anatase NPs (5.5 mM), gold tetrachloride (2 mM), and methanol (12.34 M), at pH 3.5.

Finally, we analyzed the interface between TiO_2 NPs and metal NDs with High Resolution TEM, as this contact is essential when considering NHDs as photocatalysis bricks. The as-prepared anatase polyhedral TiO_2 NPs are single crystals enclosed by mainly {101} and {001} low index facets as predicted by Wulff theory and confirmed by atomistic models.[43-44] These surfaces are mostly rough and made of terraces, valleys and steps (

Figure b and 4c).

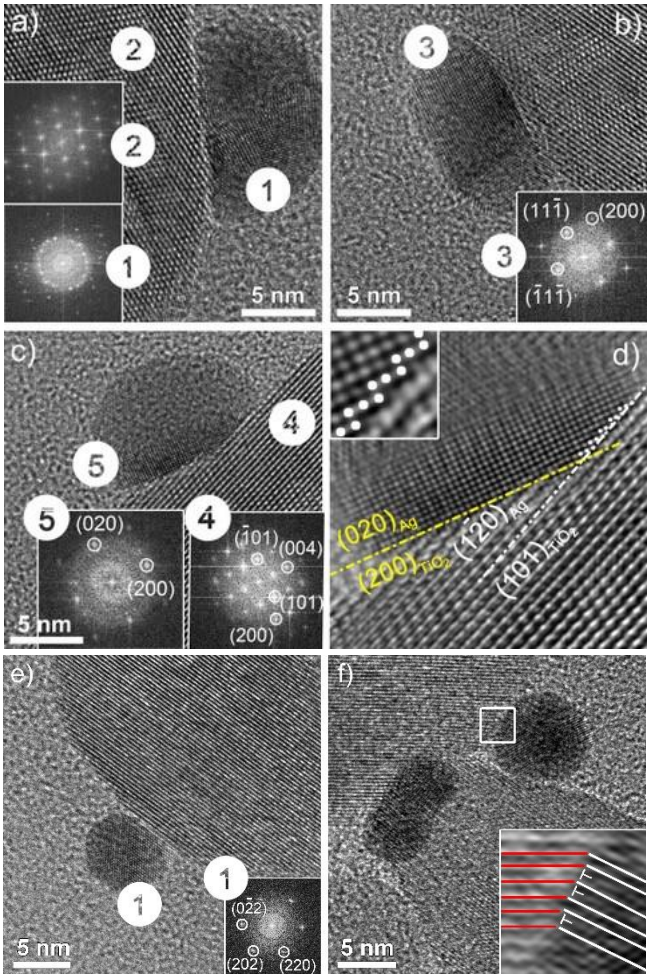

Figure 4. a-c) HRTEM micrographs illustrating the variety of TiO_2/Ag interfaces with the corresponding digital diffractograms of the labeled zones. d) Higher magnification of image c with zoom-in inset of (020) and (200) Ag stepped interface. e-f) HRTEM micrographs of TiO_2/Au interfaces and the corresponding digital diffractograms of the labeled zone. A dislocation network zoom is presented on inset of f), noted as ⊥.

The metals, either silver or gold, are found to be deposited as single nanosized clusters onto both {110} and {200} TiO_2 facets and on the three types of sites which involve flat terraces, concave and convex surfaces. Typical high-resolution TEM (HRTEM) micrographs sitting at the interface between silver, or gold, deposited NDs and their oxide support are shown on Figures 4a-d and 4e-f. Metal clusters can either exhibit monocrystalline character (Figure 4e),

be twinned (Figure 4f) or composed of disoriented domains as illustrated by the complex digital diffractogram of Figure 4a. Figure 4 shows HRTEM images where the incident electron beam is parallel to the [011], [001] and [$\bar{1}$11] axis of the gold or silver structures presenting a {111}, {001} or {110} interface plane with the TiO_2 support (similar orientation relationships have already been observed for silver and gold deposited onto other support oxides such as MgO and CeO_2).[45-46]

One can also note on Figure 4d that for a same silver cluster, the interface with TiO_2 can be flat – $(020)_{Ag}$ // $(200)_{TiO2}$ – or stepped: $(101)_{TiO2}$ parallel to $(1\bar{2}0)_{Ag}$ mean plane with $(020)_{Ag}$ and $(200)_{Ag}$ steps. Such microstructural features seem to be induced by TiO_2 NPs surface defects in order to elastically reduce the interfacial strains and favor heterogeneous nucleation. Another way for the softer material, the gold ND, to compensate for the $\Delta a/a$ interface lattice mismatch with the oxide NP is the creation of a dislocation network. It is represented by the additional reticular half-planes shown on the inset of Figure 4f. A dislocation can be seen every 2 or 3 lattice planes which is in good agreement with the evaluated misfit value of about 39%.

In order to enlighten the flexibility and the reliability of this laser-deposition method, we investigated the growth of these single metallic NDs as a function of the different parameters involved in the experiment. We tested both single and two flow microchannels, we changed the beam intensity *I*, the flow velocity *v*, and the metallic ion concentration in the bulk $[M^{n+}]_{bulk}$; the hole scavenger concentration (methanol at 50% v/v) was kept constant. Experiments were performed at pH = 3.5 with an atomic concentration $[TiO_2]$ = 5.5 mM corresponding to 10^{-8} mol/L of TiO_2 NPs characterized by a specific surface area of 46 m^2/g.[47] Results on the growth of single silver ND onto the surface of TiO_2 NPs are illustrated in Figure 5 varying only one parameter at a time.

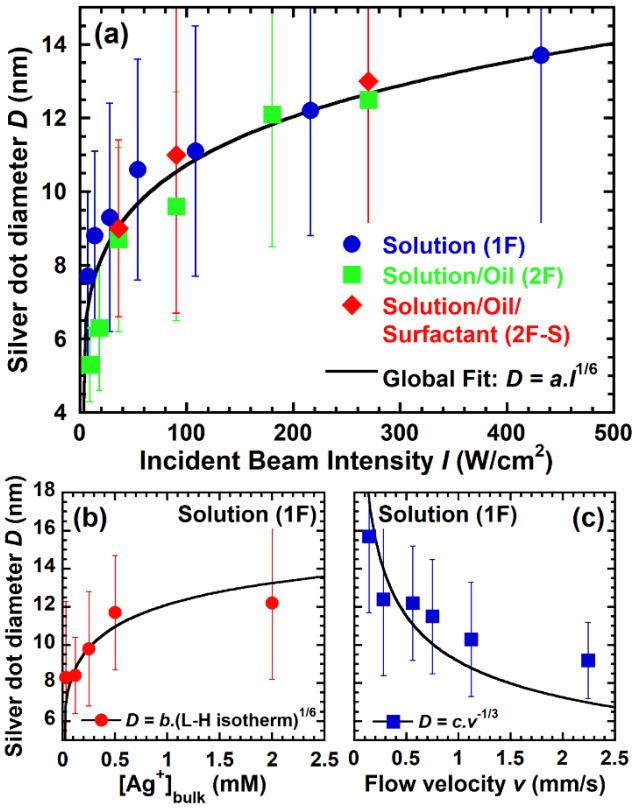

Figure 5: (a) Silver dot growth *versus* the beam intensity I onto the surface of the TiO_2 NPs in different flow conditions (one-fluid (1F) *versus* two-fluids without (2F) and with surfactant (2F-S)) for $[Ag^+]_{bulk}$ = 2 mM and v = 560 µm/s. (b) silver dots growth in the one-fluid case *versus* $[Ag^+]_{bulk}$ for I = 216 W/cm^2 and v = 560 µm/s, and (c) *versus* the flow velocity inside the microchannel for $[Ag^+]_{bulk}$ = 2 mM and I = 216 W/cm^2. See text for fit explanations.

At first, for $[Ag^+]_{bulk}$ = 2 mM and v = 560 µm/s, silver dots grow when increasing the beam intensity I, *i.e.* when increasing the rate of production of electrons available at the TiO_2 surface (Figure 5a); note that the growth law is not affected by the type of flow inside the microreactor (one *versus* two liquids) nor by the presence of surfactant. Then, for I = 216 W/cm^2 and v = 560 µm/s, the silver ND growth depends on the silver nitrate bulk concentration, *i.e.* on the concentration $[Ag^+]_{ads}$ of silver ions adsorbed at the TiO_2 surface (Figure 5b). Finally, for $[Ag^+]_{bulk}$ = 2 mM and I = 216 W/cm^2, the silver dot size decreases when increasing the flow velocity v, *i.e.* when decreasing the exposure time t_{exp} in the laser beam (Figure 5c). Yields in TiO_2/Ag NHDs synthesis remain stable around 90%.

Silver ND growth modelling & confrontation to experiments

In view of the robustness of the laser-deposition at the nanoscale, we developed a growth model of silver NDs from $[Ag^+]_{ads}$ on semiconductor substrates to probe quantitatively the observed behaviors and see if it is possible to capture general mechanisms for a predictive approach of NDs photodeposition driven by lasers.[10] The extension to metal ions M^{n+}, of degree of oxidation $n \neq 1$, is discussed in the subsequent section, experimentally and theoretically illustrated for $n = 3$ in the case of gold laser-deposition.

Kinetics equations and solution for the production of Ag^0

Upon light absorption within the band gap of TiO_2 NPs, electron-hole pairs are produced in the bulk and at the surface at a rate g proportional to αI, where α is the optical absorption of the solution at the considered wavelength (see Supporting Information S4 for the calculation of α from the absorption cross-section). The electrons, with a concentration [e], either recombine with holes at a rate k_r, or are trapped on defects (effect that can be neglected due to the large amount of carriers produced with a focused laser), or reduce Ag^+ ions adsorbed at the surface of TiO_2 with an effective rate k_e. In the same way, holes, with a concentration [h], may recombine with electrons, or be trapped on defects (effect still neglected due to the large amount of carriers produced) or may oxidize the hole scavenger HS (here methanol) adsorbed at the surface of TiO_2 with a rate k_h. These different steps are summarized by eq 1:

$$\left[TiO_2 + h\nu \xrightarrow[k_r]{g} TiO_2\left(e^-, h^+\right) \right]_{bulk}, \quad (1a)$$

$$\left[HS + h^+ \xrightarrow{k_h} HS^+ \right]_{surface}, \quad (1b)$$

$$\left[Ag^+ + e^- \xrightarrow{k_e} Ag^0 \right]_{surface}, \quad (1c)$$

where some measured values of these kinetic parameters extracted from the literature and other deduced from our investigation, are compiled in Table 2.

Table 2. Kinetic parameters published in the literature and fitted/obtained in the present work:

	Parameter	Value	Reference
TiO_2-P25	k_r ($M^{-1}.s^{-1}$)	(7.2±0.6) 10^9	Ref. [48]
TiO_2-P25/Pt(0)	k_r ($M^{-1}.s^{-1}$)	1.8 10^9	Ref. [48]
TiO_2 Anatase/Ag(0)	k_r ($M^{-1}.s^{-1}$)	(1.04±0.06) 10^9	This work: fitted from Ag^0 ND growth on TiO_2
TiO_2/MeOH	k_h ($M^{-1}.s^{-1}$)	1.4 10^9	Ref. [49]
TiO_2-P25/MeOH	K_{HS} (M^{-1})	1118.1	Ref. [50]
	n-OH^-/nm^2	4.6-4.8	Ref. [51]
TiO_2/Ag^+	k_e ($M^{-1}.s^{-1}$)	(3.54±0.2) 10^4	Ref. [52]
TiO_2-P25/Ag^+	K_{Ag} (M^{-1})	205	Ref. [53]
	n-Ag^+/nm^2	2.3	Ref. [53]
TiO_2-P25/Au^{3+}	k_e ($M^{-1}.s^{-1}$)	(0.3-1.0) 10^4	Ref. [54]
TiO_2/Au^{3+}	k_e($M^{-1}.s^{-1}$)	1.18 10^6	Predicted in Ref.[55]
TiO_2 anatase/Au^{3+}	k_e($M^{-1}.s^{-1}$)	(4.45±0.7) 10^4	This work: fitted from Au^0 ND growth on TiO_2
TiO_2/Au^{3+}	K_{Au} (M^{-1})	(250±100)	Fitted from Ref. [56]
	n-Au^{3+}/nm^2	(2.11±0.37)	Fitted from Ref. [56]

Several hypotheses can be proposed to solve these equations (see detailed descriptions in Supporting Information S10). First, the diffusion time of the carriers inside TiO_2 NPs can be neglected when compared to the time scales involved in the NDs growth process (*i.e.* a few tens of ms, as calculated below). We can also relate the adsorbed species $[Ag^+]_{ads}$ and $[HS]_{ads}$, which react with the photoproduced electrons and holes, to their bulk values $[Ag^+]_{bulk}$ and $[HS]_{bulk}$ by Langmuir-Hinshelwood type equations.[57] Furthermore, since the later are in excess in the solution, $[Ag^+]_{ads}$ and $[HS]_{ads}$ can be assumed as constant and equal to their Langmuir-Hinshelwood equilibrium values all along the laser-deposition process so that we can reduce the order of the chemical reactions by setting $k'_e = k_e \left[Ag^+ \right]_{ads}$ and $k'_h = k_h \left[HS \right]_{ads}$. We finally state that the number of electron-hole pairs is preserved during the entire laser-deposition process ($d\left[e\right]/dt = d\left[h\right]/dt$), which is again coherent when looking at the time scales associated to the light exposure. Using the above hypotheses, the time-dependent variation of the electron concentration [e] becomes:[58]

$$[\mathrm{e}](t) = \frac{2g}{k'_{\mathrm{e}}} \frac{1}{1+\sqrt{\beta}\,coth(t/\tau)} \tag{2}$$

where $\beta = 1 + \frac{4k_{\mathrm{r}}g}{k'_{\mathrm{h}}k'_{\mathrm{e}}}$, $g = \alpha I \Big/ \left(10^3 N_{\mathrm{A}} \left(hc/\lambda_0\right)\right)$ is rate of production of electrons expressed in M.s^{-1}, hc/λ_0 is the photon energy and N_{A} is the Avogadro number. $\tau = 2\Big/\left(k'_{\mathrm{e}}\sqrt{\beta}\right)$ is the associated time scale. Eq 2 allows to find the production of [Ag^0] at the surface of TiO_2 NPs. The solution $\beta = 1$ corresponds to an asymptotically 'low field' situation where g vanishes, likely relevant for a photodeposition process driven by a UV lamp (see detailed descriptions in Supporting Information S10).

While using focused lasers, we can instead investigate the 'high field' case corresponding to $\beta >> 1$. In this case, $\tau = \sqrt{k'_{\mathrm{h}}/k_{\mathrm{r}}k'_{\mathrm{e}}\,g}$ and we find:

$$[\mathrm{Ag}](t) \approx \frac{k'_{\mathrm{h}}}{k_{\mathrm{r}}} ln\left[cosh\left(\frac{t}{\tau}\right) \Big/ exp\left(\frac{t}{\tau\sqrt{\beta}}\right)\right], \tag{3}$$

which behaves at late stage $t >> \tau$ as $[\mathrm{Ag}]_{t/\tau>>1} \approx \frac{k'_{\mathrm{h}}}{k_{\mathrm{r}}}\frac{t}{\tau} = \sqrt{\frac{k'_{\mathrm{h}}k'_{\mathrm{e}}\,g}{k_{\mathrm{r}}}}t$. Considering a beam intensity of I = 216 W/cm^2 as in Figure 5b-c, our usual conditions $[Ag^+]_{bulk}$ = 2mM and $[HS]_{bulk}$ = 12.34 M leading to $[Ag^+]_{ads}$ = 2.5 10^{-2} mM and $[HS]_{ads}$ =1.5 10^{-1} mM, respectively, and using data from Table 2, we finally get a time scale of $\tau \approx 32$ ms. This value shows that the measurements of the silver ND growth belong reasonably to the 'late-stage' regime as the exposure times mainly used in the experiments are t_{exp}= 0.13-0.2 s ($t/\tau \approx$ 4-6).

Silver nanodot growth law and first comparison to experiments

The determination of the growth law of the metallic ND is inspired by the work by Tavassoli dedicated to dew growth on partially wetting solid substrates. [59] Assuming that individual silver atoms are sufficiently mobile at the surface of TiO_2, the ND growth may happen according to two mechanisms. The first one is driven by the diffusion of

photoproduced metal atoms at the surface of the TiO_2 NP and their further coalescence at the perimeter of the nucleated ND. In the other one, the growth is triggered by a constant flux of metal atoms at the ND perimeter due to the field gradient effect induced by and directed toward this metallic ND.[60] Flux- and diffusion-driven growths are detailed in Supporting Information S11-S12. If D denotes the diameter of an already nucleated silver ND at the surface of TiO_2, they show that the predicted late stage diffusive growth in the high field case, $D(t/\tau >> 1) \propto \left((t/\tau)^2 \Big/ ln\left((t/\tau)^2 \right) \right)^{1/3}$, is dynamically far too fast as compared to growth laws measured experimentally which present a much slower dynamics of the form $D(t/\tau >> 1) \propto (t/\tau)^{1/3}$ that can be deduced from a flux-driven mechanism. Then, the growth law of a single metallic ND nucleated at the surface of a TiO_2 NP is expected to be:

$$D^3(t >> \tau) - D_C^3 = \frac{24}{\kappa} \frac{N_A v_{Ag}}{N} \left[Ag^0 \right](t) = \left(\frac{24}{\kappa} \frac{N_A v_{Ag}}{N} \right) \frac{k'_h}{k_r} \cdot \frac{t}{\tau}, \quad (4)$$

when assuming a critical diameter $D(t=0) = D_C$, and $\left[Ag^0 \right](t=0) = [e](t=0) = 0$, t = 0 s corresponding to the time at which the laser exposure starts. This late stage behavior in the high field regime predicts that (i) the diameter D of the silver ND should behave in time as $t^{1/3}$ and (ii) the associated time scale τ should highly depend on the beam intensity, through g, and on both $[Ag^+]_{ads}$ and $[HS]_{ads}$ appearing in k'_e and k'_h. The ND diameter D should then vary as $I^{1/6}$ in beam intensity, and as $[Ag^+]_{ads}^{1/6}$ and $[HS]_{ads}^{1/6}$ in concentrations. With a correlation higher than 0.9, a power law fit $D \propto I^{1/6}$ of the data presented in Figure 5a at constant flow velocity and silver ion concentration, all corresponding to different flow conditions (one fluid *versus* two fluids with and without surfactant), nicely retrieves the prediction in beam intensity for the ND growth. This fit also shows that critical diameters D_C are extremely small and can likely be neglected when looking at ND sizes larger than a few nanometers. Moreover, using adsorption data given in Table 2, the measurements illustrated in Figure 5b

at constant beam intensity and flow velocity are quite well fitted by a power law $D \propto \left[\mathrm{Ag}^{+} \right]_{\mathrm{ads}}^{1/6}$ with a correlation around 0.9. Likewise, Figure 5c shows that the power law fit $D \propto v^{-1/3}$, related to the time spent by the NPs inside the laser beam, also offers a reasonable trend, even if not as confident as the fits in beam intensity and concentration.

Rescaled silver nanodot growth

In order to propose a general view of silver ND growth by laser-deposition onto TiO_2 NPs, we fitted our whole measurement set according to the late stage growth law given by eq 4. To do so, we used all the data compiled from the literature and given in Table 2, except the electron-hole recombination rate k_r, since a decrease is expected in presence of metal loading which favors charge separation.[48] In a first step, we calculated $[HS]_{ads}$ and $[Ag^{+}]_{ads}$ using a Langmuir-Hinshelwood description. We also use the optical absorption $\alpha = 0.337$ cm^{-1} of the TiO_2 solution (5.5 mM) in the microchannel calculated from the absorption cross section of Rayleigh TiO_2 NPs and comforted by subtracting the calculated scattering contribution[61] to the extinction measured by UV-Vis absorption (see Supporting Information S4).

In a second step, as the recombination rate k_r may depend on the metal loading on TiO_2 NPs,[48] we first injected the expression of $\tau = \sqrt{k'_h / \left(k_r k'_e \, g \right)}$ into eq 4, artificially extract $1/\sqrt{k_r}$ from its right-hand side and finally plot the cube diameter D^3 of the NDs as a function of $\left(\frac{24}{\kappa} \frac{N_A v_{Ag}}{N} \right) \sqrt{k'_h \, k'_e \, g} \, .t$ which is supposed to be linear with a slope of $1/\sqrt{k_r}$. The linear fit, with a correlation better than 0.9, gives $\left(k_r \right)_{\mathrm{Fit}} = \left(1.04 \pm 0.06 \right) 10^9$ $M^{-1}s^{-1}$. The corresponding growth law is illustrated in Figure 6a where several aspects can be enlightened. At first, it is clearly demonstrated that experiments performed in different flow conditions, and for varying beam intensities, silver ion concentrations and flow velocities, indicated by the different color sets, all rescale together onto a single 'master curve'. Then, the $D\left(t >> \tau \right) \propto \left(t/\tau \right)^{1/3}$ behavior

expected at high field for a late stage ND growth driven by a constant flux of silver atoms is perfectly retrieved over more than one order of magnitude in rescaled time. For comparison, we also plotted the expected ND growth without any fitting parameter and using instead the values of the recombination rates k_r published for both raw and metal-loaded TiO_2 NPs (see Table 2).[48] Our value is almost one order of magnitude smaller than that measured for raw TiO_2 ($k_r = (7.2 \pm 0.6) 10^9$ $M^{-1}s^{-1}$) in good agreement with the well-established statement that metal loading decreases the recombination rate k_r due to the electron attraction towards the metallic ND, and our k_r value is even smaller than that obtained from classical metal-loading ($k_r = 1.8\ 10^9$ $M^{-1}s^{-1}$) since our metal loading is larger and better organized than before.[48]

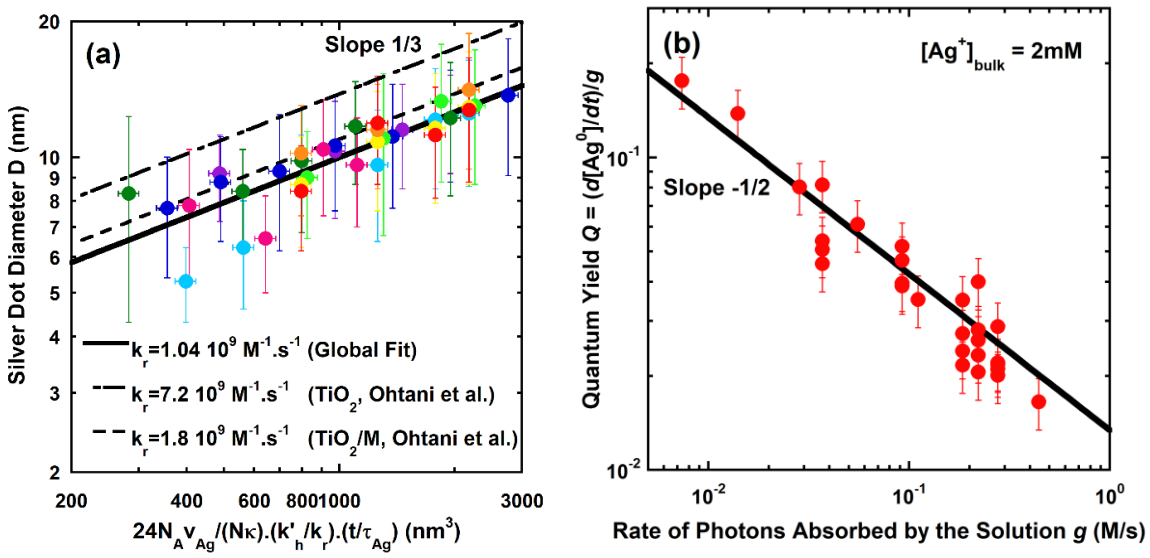

Figure 6: a) Plot as a function of the reduced time t/τ of the silver ND growth obtained for varying flow-parameter conditions (1/2F/2FS-parameter); purple: 1F-Velocity at $I = 216$ W/cm^2 and $[Ag^+]_{bulk} = 2$ mM, deep blue: 1F-Intensity at $v = 560$ µm/s and $[Ag^+]_{bulk} = 2$ mM, Sky blue: 2F-Intensity at $v = 560$ µm/s and $[Ag^+]_{bulk} = 2$ mM, dark green: 1F-Concentration at $I = 216$ W/cm^{2}and $v = 560$ µm/s, green: 2FS-Intensity at $v = 560$ µm/s and $[Ag^+]_{bulk} = 2$mM, yellow: 1F-Intensity at $v = 560$ µm/s and $[Ag^+]_{bulk} = 2$mM, orange: 2FS-Intensity at $v = 560$ µm/s and $[Ag^+]_{bulk} = 2$mM, pink: 2FS-Intensity at $v = 560$ µm/s and $[Ag^+]_{bulk} = 0.4$ mM, red:

2FS-Intensity at v = 560 µm/s and $[Ag^+]_{bulk}$ = 2mM. The continuous line represents the predicted quantitative behavior using a global fit for the determination of the recombination rate k_r. Dash-dotted and dashes lines represent predictions when plotted using instead the recombination rates extracted from the literature for raw and metal-loaded TiO_2, respectively.[48] b) Variation of the experimental quantum yield for $[Ag^+]_{bulk}$ = 2 mM as a function of the rate of photon absorbed by the TiO_2 solution (see Supporting Information S13 for the evaluation of the errors bars).

At the end of this comparison between experiments and predictions it is important to check back the coherence of some hypotheses of the model. At first, working typically with beam intensities in between 50 and 400 W/cm^2, our modelling gives a ratio of exciton per absorbed photon within the range $0.12 < [e]_{steady} / (gt_{exp}) < 0.35$ when integrated over the exposure time. Then, the high field condition used to interpret the data (*i.e.* $k_r [e] / k'_h >> 1$, see Supporting Information S10) leads to the condition $I >> 0.17$ W/cm^2 for $[Ag^+]_{bulk}$= 2 mM, which is also very well satisfied.

As a final point of interest, we analyzed the quantum efficiency of the laser-deposition process. By definition, the quantum yield Q is equal to the ratio of the reaction rate of interest (here $d[Ag^0]/dt$) to the efficient photonic flux, *i.e.* the rate of photodeposited silver divided by the rate of electron-hole pair production resulting from photon absorption by the solution: $Q = \left(d[Ag^0]/dt\right)/g$. As $D^3(t >> \tau) \approx \frac{24}{\kappa}\frac{N_A v_{Ag}}{N}[Ag^0](t)$ (see eq 4), we find:

$$Q = \frac{0.9N}{N_A v_{Ag}} \frac{\kappa}{24} \frac{D^3}{gt}, \qquad (5)$$

making use of the linearity of D^3 with time and multiplying by 0.9 to take into account the 90% experimental yield in NHDs. Q can then be experimentally determined from the NDs

diameter measurements obtained at given beam intensity and exposure time. Using eq 4 for the expression of D^3, Q can as well be expressed as:

$$Q = 0.9\sqrt{k'_h\, k'_e/(g k_r)}, \qquad (6)$$

which shows that the quantum yield Q should behave as $Q \propto 1/\sqrt{g}$. Figure 6b illustrates this variation for our set of measurements at the most used concentration $[Ag^+]_{bulk}$= 2mM. A power law fit gives $Q_{fit} = (1.34 \pm 0.05)10^{-2}/\sqrt{g}$ in good agreement with the expected scaling and with an amplitude slightly larger than the one predicted from Table 2, our estimation of k_r in presence of a single ND and eq 6 ($Q = 1.18\ 10^{-2}/\sqrt{g}$), but largely within the relative error of 19 % calculated from the relative errors already used for the investigation of the growth law of NHDs. Then, for typical conditions, I = 216 W/cm^2 and $[Ag^+]_{bulk}$ = 2 mM, the quantum yield is $Q \approx$ 2.9%, showing that the laser deposition method offers quite reasonable values.

Gold nanodot growth

In order to strengthen our predictions on metallic ND growth onto TiO_2 NPs based on mobile metallic atoms produced by photoreduction, we extended our investigation to the gold deposition. Experiments were performed in the same way as those involving silver laser-deposition by varying beam intensity *I*, flow velocity *v* and gold precursor concentration $[Au^{3+}]_{bulk}$, here dissolved gold tetrachloride; we also used the same type of microchannels and the same setup. The initial concentrations of $[TiO_2]$ = 5.5 mM (polyhedrons of mean typical sizes 25x25x40 nm^3) and methanol (50% v/v) at pH = 3.5 are also identical to those used for laser-deposition of silver.

Kinetics equations and gold nanodot growth

While our growth model at the surface of TiO_2 can easily be generalized mathematically to the reduction of metal ions M^{n+}, of degree of oxidation n, when hypothesizing that the n

electrons required for the reduction to M^0 are 'transferred concomitantly', such an oversimplified point of view is usually far from the reality. A set of coupled reactions needs indeed to be solved in order to describe the global scheme $'M^{n+} + ne^- \rightarrow ... \rightarrow M^0'$, preventing a rigorous definition of a simple reaction rate. This is particularly true for the reduction of Au^{3+} which involves three stages, photoreduction of Au^{3+} to Au^{2+}, disproportionation of two Au^{2+} in Au^{3+} and Au^+ and finally photoreduction of Au^+ to Au^0;[62] note that this mechanism is still the subject of important research, in particular when characterizing nucleation and growth of gold NPs in solutions.[63-65] Nonetheless, investigations of the photoreduction of Au^{3+} in the presence of TiO_2-anatase[66] and P25[67] show that the photoreduction of Au^{3+} to Au^0 can be assimilated to the pseudo first-order net reaction $'Au^{3+} + 3e^- \xrightarrow{k_e} Au^0'$ when investigating its kinetics over time scales long compared to those involved in the photoreduction mechanism. This statement should therefore apply here when considering the time scale for the growth of gold NDs. Then, the late stage growth dynamics of a gold ND on a TiO_2 NP in the high field case is expected to be described by equations analogous to those used for the production of silver atoms and for the growth of a silver ND. Consequently, a gold ND should grow at the surface of TiO_2 according to:

$$D^3\left(t >> \tau\right) - D_C^3 = \left(\frac{24}{\kappa}\frac{N_A v_{Au}}{N}\right)\frac{k'_h}{k_r}\cdot\frac{t}{\tau}, \qquad (7)$$

with $\tau = \sqrt{k'_h/\left(k_r k'_e\, g\right)}$ the characteristic growth time scale; v_{Au} is the volume of a gold atom. We thus expect again that (i) the diameter D of a gold ND grows as $t^{1/3}$ in time, $I^{1/6}$ in beam intensity, and as $[Au^{3+}]_{ads}^{1/6}$ and $[HS]_{ads}^{1/6}$ in concentration. The concentration of gold ions $[Au^{3+}]_{ads}$ adsorbed at the TiO_2 surface may as well be described by a Langmuir-Hinshelwood type model using data given in Table 2.

In order to present a general view of the gold ND growth by laser-deposition onto the TiO_2 NPs, we used the same procedure as in the silver ND growth case by fitting the whole

experimental set according to the late stage growth law given by eq 7. In a first step, we used all the data extracted from the literature given in Table 2, including the electron-hole recombination rate k_r deduced from the growth of a single silver ND since reaction rates and adsorption properties are quite similar (see Table 2). In a second step, as we found from the literature two orders of magnitude difference in the values for the pseudo first-order rate k_e for the gold reduction at the surface of TiO_2 (see Table 2), we injected the expression of τ into eq 7, artificially extract $\sqrt{k_e}$ from the right-hand side and plot again the NDs cube diameter as a function of $\left(\frac{24}{\kappa}\frac{N_A v_{Ag}}{N}\right)\sqrt{\frac{k'_h\left[Au^{3+}\right]_{ads} g}{k_r}}.t$ which is supposed to be linear with a slope $\sqrt{k_e}$. A linear fit gives $(k_e)_{Fit} = (4.45 \pm 0.7)10^4$ $M^{-1}s^{-1}$. The corresponding growth law is illustrated in Figure 7a. Several aspects can be raised. At first, it clearly appears that the experiments performed for different concentrations of the gold ion salt and at different beam intensities continue to rescale together onto a single 'master behavior', even if data are slightly noisier than in the silver case (likely related to the more complex reduction scheme).

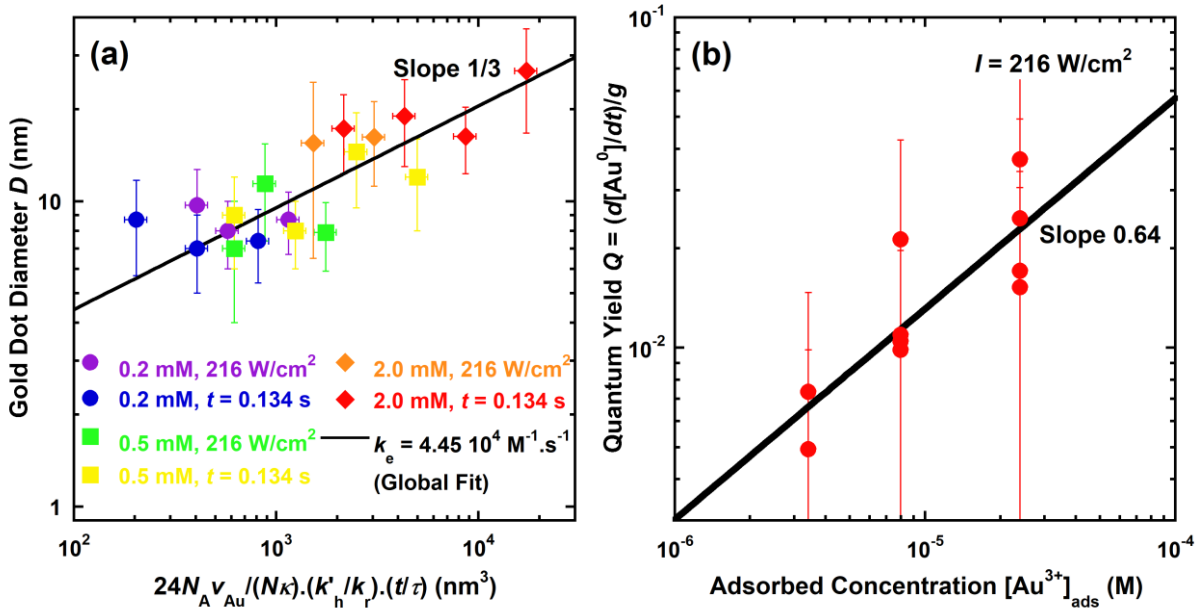

Figure 7: a) Plot in reduced time of the gold ND growth obtained under various conditions specified in the legend. All the experiments were performed in a one-fluid microchannel. The

continuous line represents the expected quantitative behavior using a global fit for the determination of the effective reaction rate k_e. b) Variation of the experimental quantum yield Q for I= 216 W/cm^2 as a function of the gold ion concentration adsorbed at the surface of TiO_2. See Supporting Information S13 for the evaluation of the errors bars.

Then, the $D(t >> \tau) \propto (t/\tau)^{1/3}$ behavior expected at high field for the late stage ND growth driven by a constant flux of gold atoms is retrieved over almost two orders of magnitude in rescaled time. Most of the experiments being performed at I = 216 W/cm^2 and [Au^{3+}] = 2 mM, the growth time scale $\tau = \sqrt{k'_h/(k_r k'_e g)} \approx 29$ ms is five time smaller than our mainly used laser exposure so that the condition $t >> \tau$ is reasonably well verified. Moreover, $I >> 0.21$ W/cm^2 so that the high field condition $k_r[e]/k'_h >> 1$ is also perfectly fulfilled. Finally, our deduction of a pseudo first-order reaction rate $(k_e)_{Fit} = (4.45 \pm 0.9)10^4$ $M^{-1}s^{-1}$ at the surface of the TiO_2 reinforces the range of scarce available literature data since it is in between a smaller value obtained from a TiO_2-P25 gold-methanol solution illuminated with a UV led at 375 nm ($k_e \in [0.3\text{-}1.0]$ 10^4 $M^{-1}s^{-1}$ when varying either $[HS]_{bulk}$ or [TiO_2-P25]),[67] and a larger one predicted for TiO_2 anatase ($k_e = 1.18$ 10^6 $M^{-1}s^{-1}$).[52]

The final aspect to consider is the quantum yield $Q = \left(d\left[Au^0\right]/dt\right)/g$ corresponding to the gold laser-deposition. On the one hand, we have $Q = \frac{0.5N}{N_A v_{Au}} \frac{\kappa}{24} \frac{D^3}{gt}$, due to the linearity in time of D^3 and the experimental yield in NHDs of 50%; it can be determined experimentally from the measurements of the ND diameters obtained for different beam intensities and exposure times. On the other hand, focusing on the concentration $\left[Au^{3+}\right]_{ads}$ effects, we also get the expression $Q = 0.5\sqrt{k'_h k_e \left[Au^{3+}\right]_{ads}/(gk_r)}$ and expect $Q \propto \left[Au^{3+}\right]_{ads}^{1/2}$ at fixed beam intensity I. As experimentally illustrated in Figure 7b, the quantum yield indeed increases

with $\left[Au^{3+}\right]_{ads}$ at the surface of TiO_2, but data are much noisier than those obtained for the silver deposition and grow faster than the expected scaling since a power law fit gives an exponent 0.64 instead of 0.5. The relative error on Q is ≥ 24% giving an exponent 0.5 loosely compatible. The main conclusion is that in our typical conditions, I = 216 W/cm^2 and $[Au^{3+}]_{bulk}$ = 2mM, the mean quantum yield is 2.2% and thus slightly smaller than that obtained for silver deposition (2.9%) showing that gold laser-deposition seems slightly less efficient.

Model confrontation to growth data from the literature

Despite the importance of metal loaded semiconducting metal oxide NPs in many applications including photocatalysis, as far as we know very few publications tried to investigate in details the metallic NDs growth onto TiO_2 NPs. Experiments were all performed using a UV lamp with variable exposure times. Lu *et al.*[17] used a solution composed of TiO_2 nanorods suspended in toluene and a mixture of silver nitrate and oleylamine. Using a 6 W UV lamp (wavelength 365 nm) positioned at 10 cm of the reaction vial, they produced NHDs with a single Ag^0 ND per nanorod. Experiments were performed by varying the exposure time for three concentrations in hole scavenger, 1-hexadecanol, from zero (in this case oleylamine likely played this role) to low (0.1 mM) and high (0.5 mM) concentrations and they found slightly shifted growth laws (see Inset of Figure 8). Considering the involved exposure time (from 30 to 600 min) we can confidently foresee a growth law in the late stage regime, either $D^3 \propto t$ in the low field case (see Supporting Information S11), or $D^3 \propto \sqrt{[HS]_{ads}}t$ at high field (see eq 4), all other parameters being constant. These raw data should then behave as $D \propto t^{1/3}$, and this is effectively the case as confirmed by the fits represented in the inset of Figure 8; the correlations are 0.99, 0.99 and 0.92 respectively for 0, 0.1 and 0.5 mM of hexadecanol. Also, since there is a dependence in

hole scavenger concentration, a high field situation is counter-intuitively hypothesized despite the quite low photon density expected from their UV lamp and size of the vial. Due to missing elements for a quantitative interpretation, for instance on how to determine $[HS]_{ads}$, we supposed that the $[HS]_{bulk}$ they used were sufficiently low to linearly approximate the expected Langmuir-Hinshelwood behavior (*i.e.* $[HS]_{ads} \propto [HS]_{bulk}$). Moreover, hole scavenging cannot be zero due to the electric charge equilibrium so that oleylamine may as well play this role in the absence of hexadecanol. Consequently, we first plotted $D^3 \propto \sqrt{[HS]_{ads}}\,t \propto \sqrt{[HS]_{bulk}}\,t$ for low (0.1 mM) and high (0.5 mM) hexadecanol concentrations. As shown in Figure 8, they both collapse quite well on a single linear behavior. Then, by forcing the collapse of the growth in the absence of hexadecanol onto the common behavior obtained for 0.1, 0.5 mM hexadecanol, we finally find that a whole collapse onto the same 'master behavior' (Figure 8) imposes a hole scavenger concentration $[HS]_{bulk} = 0.05$ mM associated to the presence of oleylamine in the solution; the correlation is 0.93.

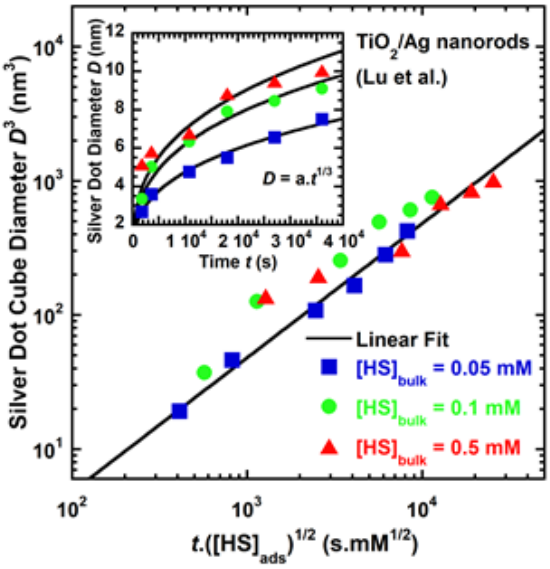

Figure 8. Rescaling of the silver ND growth at the surface of TiO_2 nanorods investigated by Lu *et al.*[17] as a function of the exposure time to a UV lamp for three hole scavenger concentrations. Inset: row data fitted with a power law $D \propto t^{1/3}$.

The conclusion is that Lu's measurements can be interpreted with our model and its consistency is now illustrated 'in reverse' by finding a very low hole scavenging concentration, as expected in the absence of hexadecanol, from the predicted collapse onto a single master behavior.

To the best of our knowledge, photo-induced single gold ND growth on TiO_2 NPs is almost not documented. We are just aware of a data set obtained by Chang *et al.*[68] using 10 W UV lamps (245 nm) or a 400 W high pressure mercury lamp with chloroauric acid as Au^{3+} precursor and commercially available TiO_2-P25; this data set is too weak to be reasonably analyzed. Growth of photodeposited gold ND has nonetheless been investigated on II-VI semiconductors NPs. For instance Carbone *et al.*[16] investigated the gold deposition on one side of CdS and CdSe(core)/CdS(shell) nanorods using an ordinary UV lamp (2-3 mW/cm^2) with chloroauric acid as the gold precursor and ethanol as the hole scavenger; a chloroform solution of $HAuCl_4$, (di-*n*-dodecyl) dimethyl ammonium bromide (DDAB), and dodecylamine (DDA) was injected dropwise. The authors measured the mean diameter of the gold NDs at exposure times 2, 5, 11, 30, 60, 90, and 120 min and showed that the volume of the NDs increased linearly with time, as expected from our model in both low and high field regimes. Since they did not vary any other parameter, we cannot go further into the comparison. Using the same protocols, Dermotière *et al.*[14] also investigated the gold deposition at the tip of CdSe/CdS nanorods using a UV lamp (1 mW/cm^2). They measured the variation of the average diameter D of the gold NDs with exposure times varying from 10 min to one hour. The fit of these data with a power law leads to a 1/3 exponent with a correlation better than 0.98, showing again an excellent compatibility with our model. Consequently, even if data sets remain scarce, it seems that the growth of single silver and gold NDs driven by UV lamps onto semiconductor NPs also follows the model expectations.

CONCLUSION

Considering the difficulty to obtain metal-metal oxide semiconductor NHDs in a general way, and in particular when setting a photodeposition approach, we demonstrated that the implementation of focused lasers for the production of electron-hole pairs in TiO_2 NPs is tremendously more efficient than the use of UV lamps and allows the formation of heterodimers. From this study, it clearly appears that, what primarily matters for the synthesis of NHDs is the rate of production of electron-hole pairs and not the number of pairs which is produced. To demonstrate this change of paradigm, (i) we built and characterized a dedicated optofluidic setup in which a bar of laser light crosses a flowing suspension composed of TiO_2 NPs, a metallic salt and a hole scavenger, (ii) we varied the beam intensity, the metallic salt and its concentration, and the flow velocity of the solution to change the time exposure. (iii) Under such conditions, we not only optically produced and structurally characterized NHDs, but also developed a model for the growth of the metallic dot onto the surface of a TiO_2 NP. (iv) We quantitatively compared predictions to measurements of silver and gold NDs obtained in various tested conditions, (v) we characterized the associated quantum yield, and finally (vi) we confronted our model to experimental data extracted from the literature on silver and gold ND growth driven by UV lamps on TiO_2 and also on II-VI semiconducting NPs. The main conclusion is that, beyond giving access to a huge flux density of photons, and thus to large rates of electron-hole pair production, as a sort of corner stone for NHDs synthesis, focused laser waves also offer a fine control on optical excitation, which allows a quantitative confrontation to models and the emergence of predictable master behaviors for photodeposition synthesis at the nanoscale.

METHODS

Chemicals: Titanium(IV) isopropoxide (TIPO, 97%), triethanolamine (TEOA, ≥99%), oleic acid (OA, 90%), sodium hydroxide (NaOH, 99.99%), silver nitrate ($AgNO_3$,99%), potassium

gold(III) chloride ($KAuCl_4$, 99.995%), methanol (anhydrous, 99.8%), dodecane (99%), heptane (99%), Sorbitane monooleate (SPAN80), trichloro(octadecyl)silane (TOS, ≥90%), isooctane (anhydrous, 99.8%) and chloroform (anhydrous, ≥99%) were purchased from Sigma Aldrich and used as-received without further purification. The deionized water (18.2 MΩ·cm) was obtained with Milli-Q filtration station.

Materials: A ThermoFisher Scientific K-ALPHA spectrometer was used for XPS surface analysis with a monochromatized AlKα source (hν=1486.6eV). The Powdered samples were pressed onto small indium foils or directly examined on TEM grids with a 200 microns X-Ray spot size. The full spectra (0-1100 eV) were obtained with a constant pass energy of 200eV and high resolution spectra at 40eV. Charge neutralization was applied during analysis and sputtering was achieved with argon ions. High resolution spectra were quantified and/or fitted using the AVANTAGE software provided by ThermoFisher Scientific (Scofield sensitivity factors used for quantification). The phase identification of the samples was performed with X-ray diffraction (XRD) using a powder diffractometer (PANalytical X'Pert Pro) equipped with Cu Kα1 radiation, λ = 1.540598 Å. Samples for transmission electron microscopy (TEM) were prepared by suspending the Au/TiO_2 and Ag/TiO_2 powders in alcohol by ultrasonication and depositing a drop of the suspension on a copper grid covered with a carbon film. The grid was finally air-dried for 15 min. TEM and high-resolution TEM (HRTEM) observations were performed using a JEOL 2200 FS equipped with a field emission gun, operating at 200 kV and with a point resolution of 0.23 nm. High-resolution transmission electron microscopy micrographs and videos were acquired with a GatanUltrascan CCD 2k-2k and digital diffractograms were calculated using the Gatan Digital Micrograph program. Moreover, in order to be representative and statistically meaningful, many images from several regions of various samples were recorded and the most characteristic results are presented here, and at

least 200-250 NPs were treated. The UV-vis absorption spectra were recorded with 3600 Shimadzu UV-Vis-NIR spectrophotometer using 1cm quartz cuvettes.

Synthesis of TiO_2: TiO_2 nanomaterials were prepared according to the method published elsewhere.[28, 69] First, 0.1 mol of TIPO and 0.2 mol of TEOA were mixed under argon flow and stirred at room temperature for 24h. Then, 144 mL of deionized water was added giving a stock solution with $C(Ti^{4+}) = 0.5$ mol/L. Then, for TiO_2 nanoparticles preparation, 10 mL of the stock solution were diluted with deionized water up to 20 mL (pH=9.4; $C(Ti^{4+}) = 0.25$mol/L) in 35 mL glass bottle and aged at 100 °C for 24h. After that, the solution was directly transferred into Teflon-lined autoclave and aged at 140 °C for 72h. Finally, the autoclave was cooled down to room temperature and the product was collected by centrifugation at 15,000 rpm for 45 min. The precipitated product was washed for several times with NaOH solutions (pH = 12), 2 M HNO_3 and water (until pH = 7) by sonication/centrifugation. As-prepared TiO_2 NPs analyzed with TEM were 25x25x40 nm (Figure S1).

Preparation of the reaction solutions.

Aqueous solution phase: The reaction solution was prepared by mixing of 0.022 mmol of TiO_2 and 0.008 mmol of $AgNO_3$ in 4mL water/methanol (1v/1v) in dark under Ar. The pH was adjusted to 3.5 with 0.1M HNO_3. The concentration of TiO_2 and $AgNO_3$ in final solution was 5.5 and 2 mM, respectively; the concentration of $AgNO_3$ was also varied in between 0.03 to 8 mM for a dedicated experiment. The $KAuCl_4$ was used for gold nanoparticles photodeposition at concentration from 0.2 mM to 2 mM.

Oil phase.: The oil (*n*-dodecane) is used to set a wetting layer at the channel walls and wrap the drops of aqueous NPs solution by an organic layer when co-flowing in the square channel. This prevents the laser-deposition on the channel walls. 2%wt of nonionic surfactant SPAN80 can optionally be added in oil in order to transfer the NHDs from water into organic phase.

This option allows to skip the washing step of the final solution and to obtain a stable dispersion in nonpolar solvents (*e.g.* hexane, toluene).

ASSOCIATED CONTENT

Supporting Information

Additional data and figures are included in the Supplementary Information. These data describe the optofluidic experimental setup and characterization (SI1); the characterization of the TiO_2 anatase NPs (TEM, Zetammetry & XRD (Figure S2), the fabrication of the microfluidic reactor (SI3), the absorption and turbidity of the TiO_2 NPs suspensions inside the microchannel (SI4), the comparison of silver deposition onto TiO_2 NPs induced by a UV lamp and a UV continuous laser for a common deposited energy (SI5), the laser heating of the TiO_2 NPs solution flowing in the microchannel at 364 nm (SI6), the Energy Dispersive X-Ray spectroscopy (EDS) of the TiO_2/Ag NHDs (SI7), the XPS data on TiO_2 NPs (SI8), the long term stability of the TiO_2/Ag NHDs in solution (SI9), the modeling of the silver production at the surface of a TiO_2 NP (SI10), the modeling of growth of silver deposit at the surface of one TiO_2 NP under a flux of silver atoms (SI11), the modeling of the growth of silver deposit at the surface of one TiO_2 NP by diffusing silver atoms (SI12) and the calculations of error bars (SI13).

This material is available free of charge *via* the Internet at http://pubs.acs.org.

AUTHOR INFORMATION

Corresponding Author:

Delville M-H - *CNRS, Univ. Bordeaux, Bordeaux INP, ICMCB, UMR 5026, 87 avenue du Dr. A. Schweitzer, Pessac, F-33608, France.* http://orcid.org/0000-0001-8863-8225 Email: Marie-Helene.Delville@icmcb.cnrs.fr

Delville J-P - *Univ. Bordeaux, CNRS, LOMA, UMR 5798, 33405 Talence, France.*https://orcid.org/0000-0002-7376-9449 Email: jean-pierre.delville@u-bordeaux.fr

Notes

The authors declare no competing financial interest.

Funding Sources

The authors acknowledge the Aquitaine Region grant n° 20081304001, the China Scholarship Council for a PhD Grant to QB, Université de Bordeaux for a post-doctoral grant to IS. This project has received financial support from the CNRS through the MITI interdisciplinary programs (Action MITI: Nouveaux Matériaux 2020).

ACKNOWLEDGMENTS

All the TEM observations were performed on the microscopes of the Plateforme Aquitaine de Caractérisation des Matériaux (UMS 3626, CNRS−Univ.de Bordeaux, Pessac, France) and the Bordeaux Imaging Center. Financial support from the China Scholarship Council (CSC) of the People's Republic of China (Grant to Q.B.), the Aquitaine Region (project 20081304001), and the IDEX of the University of Bordeaux (project Laphia-Janapa 2012) are gratefully acknowledged. We also thank Mustafa Hamieh for performing very preliminary experiments on laser deposition.

REFERENCES

1. Kraeutler, B.; Bard, A. J., Heterogeneous Photocatalytic Preparation of Supported Catalysts. Photodeposition of Platinum on TiO_2 Powder and Other Substrates. *J. Am. Chem. Soc.* **1978,** *100,* 4317-4318,

2. Waiskopf, N.; Ben-Shahar, Y.; Banin, U., Photocatalytic Hybrid Semiconductor–Metal Nanoparticles; From Synergistic Properties to Emerging Applications. *Adv. Mater.* **2018,** *30*, 1706697,

3. Tada, H.; Fujishima, M.; Kobayashi, H., Photodeposition of Metal Sulfide Quantum Dots on Titanium(IV) Dioxide and the Applications to Solar Energy Conversion. *Chem. Soc. Rev.* **2011,** *40*, 4232-4243,

4. Bahnemann, D., Photocatalytic Detoxification of Polluted Waters. In *Environ. Photochem.*, Boule, P., Ed. Springer Berlin Heidelberg: Berlin, Heidelberg, 1999; pp 285-351.

5. Osterloh, F. E., Inorganic Nanostructures for Photoelectrochemical and Photocatalytic Water Splitting. *Chem. Soc. Rev.* **2013,** *42*, 2294-2320,

6. Litter, M. I., Last Advances on TiO_2-Photocatalytic Removal of Chromium, Uranium and Arsenic. *Current Opinion in Green and Sustainable Chemistry* **2017,** *6*, 150-158,

7. Lee, Y.; Kim, E.; Park, Y.; Kim, J.; Ryu, W.; Rho, J.; Kim, K., Photodeposited Metal-Semiconductor Nanocomposites and Their Applications. *J. Materiomics* **2018,** *4*, 83-94,

8. Vaneski, A.; Susha, A. S.; Rodríguez-Fernández, J.; Berr, M.; Jäckel, F.; Feldmann, J.; Rogach, A. L., Hybrid Colloidal Heterostructures of Anisotropic Semiconductor Nanocrystals Decorated with Noble Metals: Synthesis and Function. *Adv. Funct. Mater.* **2011,** *21*, 1547-1556,

9. Banin, U.; Ben-Shahar, Y.; Vinokurov, K., Hybrid Semiconductor–Metal Nanoparticles: From Architecture to Function. *Chem. Mater.* **2014,** *26*, 97-110,

10. Wenderich, K.; Mul, G., Methods, Mechanism, and Applications of Photodeposition in Photocatalysis: A Review. *Chem. Rev.* **2016,** *116*, 14587-14619,

11. Chan, S. C.; Barteau, M. A., Preparation of Highly Uniform Ag/TiO_2 and Au/TiO_2 Supported Nanoparticle Catalysts by Photodeposition. *Langmuir* **2005,** *21*, 5588-5595,

12. Dukovic, G.; Merkle, M. G.; Nelson, J. H.; Hughes, S. M.; Alivisatos, A. P., Photodeposition of Pt on Colloidal CdS and CdSe/CdS Semiconductor Nanostructures. *Adv. Mater.* **2008,** *20*, 4306-4311,

13. Menagen, G.; Macdonald, J. E.; Shemesh, Y.; Popov, I.; Banin, U., Au Growth on Semiconductor Nanorods: Photoinduced *versus* Thermal Growth Mechanisms. *J. Am. Chem. Soc.* **2009,** *131*, 17406-17411,

14. Demortière, A.; Schaller, R. D.; Li, T.; Chattopadhyay, S.; Krylova, G.; Shibata, T.; dos Santos Claro, P. C.; Rowland, C. E.; Miller, J. T.; Cook, R.; Lee, B.; Shevchenko, E. V., *In Situ* Optical and Structural Studies on Photoluminesence Quenching in CdSe/CdS/Au Heterostructures. *J. Am. Chem. Soc.* **2014,** *136*, 2342-2350,

15. Gomathi Devi, L.; Kavitha, R., A Review on Plasmonic Metal-TiO_2 Composite for Generation, Trapping, Storing and Dynamic Vectorial Transfer of Photogenerated Electrons Across the Schottky Junction in a Photocatalytic System. *Appl. Surf. Sci.* **2016,** *360*, 601-622,

16. Carbone, L.; Jakab, A.; Khalavka, Y.; Sonnichsen, C., Light-Controlled One-Sided Growth of Large Plasmonic Gold Domains on Quantum Rods Observed on the Single Particle Level. *Nano Lett* **2009,** *9*, 3710-14,

17. Lu, Q.; Lu, Z.; Lu, Y.; Lv, L.; Ning, Y.; Yu, H.; Hou, Y.; Yin, Y., Photocatalytic Synthesis and Photovoltaic Application of Ag-TiO_2 Nanorod Composites. *Nano Lett.* **2013,** *13*, 5698-5702,

18. Pacholski, C.; Kornowski, A.; Weller, H., Site-Specific Photodeposition of Silver on ZnO Nanorods. *Angew. Chem., Int. Ed.* **2004,** *116*, 4878-4881,

19. Wood, A.; Giersig, M.; Mulvaney, P., Fermi Level Equilibration in Quantum Dot−Metal Nanojunctions. *J. Phy. Chem. B* **2001,** *105*, 8810-8815,

20. Fernando, J. F.; Shortell, M. P.; Noble, C. J.; Harmer, J. R.; Jaatinen, E. A.; Waclawik, E. R., Controlling Au Photodeposition on Large ZnO Nanoparticles. *ACS Appl. Mater. Interfaces* **2016,** *8*, 14271-83,

21. Fernando, J. F. S.; Shortell, M. P.; Firestein, K. L.; Zhang, C.; Larionov, K. V.; Popov, Z. I.; Sorokin, P. B.; Bourgeois, L.; Waclawik, E. R.; Golberg, D. V., Photocatalysis with Pt-Au-ZnO and Au-ZnO Hybrids: Effect of Charge Accumulation and Discharge Properties of Metal Nanoparticles. *Langmuir* **2018,** *34*, 7334-7345,

22. Nakibli, Y.; Kalisman, P.; Amirav, L., Less Is More: The Case of Metal Cocatalysts. *J Phys Chem Lett* **2015,** *6*, 2265-8,

23. Nakibli, Y.; Mazal, Y.; Dubi, Y.; Wachtler, M.; Amirav, L., Size Matters: Cocatalyst Size Effect on Charge Transfer and Photocatalytic Activity. *Nano Lett.* **2018,** *18*, 357-364,

24. Ben-Shahar, Y.; Philbin, J. P.; Scotognella, F.; Ganzer, L.; Cerullo, G.; Rabani, E.; Banin, U., Charge Carrier Dynamics in Photocatalytic Hybrid Semiconductor–Metal Nanorods: Crossover from Auger Recombination to Charge Transfer. *Nano Lett.* **2018,** *18*, 5211-5216,

25. Ben-Shahar, Y.; Scotognella, F.; Kriegel, I.; Moretti, L.; Cerullo, G.; Rabani, E.; Banin, U., Optimal Metal Domain Size for Photocatalysis with Hybrid Semiconductor-Metal Nanorods. *Nature Commun.* **2016,** *7*, 10413,

26. Nakato, Y.; Tsubomura, H., Structures and Functions of Thin Metal Layers on Semiconductor Electrodes. *J. Photochem.* **1985,** *29*, 257-266,

27. Gerischer, H., A Mechanism of Electron Hole Pair Separation in Illuminated Semiconductor Particles. *J. Phy. Chem.* **1984,** *88*, 6096-6097,

28. Kanie, K.; Sugimoto, T., Shape Control of Anatase TiO_2 Nanoparticles by Amino Acids in a Gel-Sol System. *Chem. Commun.* **2004**, 1584-1585,

29. Peltonen, L.; Hirvonen, J.; Yliruusi, J., The Behavior of Sorbitan Surfactants at the Water–Oil Interface: Straight-Chained Hydrocarbons from Pentane to Dodecane as an Oil Phase. *J Colloid Interface Sci.* **2001,** *240*, 272-276,

30. Mogal, S. I.; Gandhi, V. G.; Mishra, M.; Tripathi, S.; Shripathi, T.; Joshi, P. A.; Shah, D. O., Single-Step Synthesis of Silver-Doped Titanium Dioxide: Influence of Silver on Structural, Textural, and Photocatalytic Properties. *Ind. Eng. Chem. Res.* **2014,** *53*, 5749-5758,

31. Chu, D.; Younis, A.; Li, S., Direct Growth of TiO_2 Nanotubes on Transparent Substrates and Their Resistive Switching Characteristics. *J. Phys. D: Appl. Phys.* **2012,** *45*, 355306,

32. Kaspar, T. C.; Droubay, T.; Chambers, S. A.; Bagus, P. S., Spectroscopic Evidence for Ag(III) in Highly Oxidized Silver Films by X-Ray Photoelectron Spectroscopy. *J. Phy. Chem. C* **2010,** *114*, 21562-21571,

33. Wu, Y.; Liu, H.; Zhang, J.; Chen, F., Enhanced Photocatalytic Activity of Nitrogen-Doped Titania by Deposited with Gold. *J. Phy. Chem. C* **2009,** *113*, 14689-14695,

34. Zhang, H.; Wang, G.; Chen, D.; Lv, X.; Li, J., Tuning Photoelectrochemical Performances of Ag−TiO_2 Nanocomposites *via* Reduction/Oxidation of Ag. *Chem. Mater.* **2008,** *20*, 6543-6549,

35. Arabatzis, I. M.; Stergiopoulos, T.; Bernard, M. C.; Labou, D.; Neophytides, S. G.; Falaras, P., Silver-Modified Titanium Dioxide Thin Films for Efficient Photodegradation of Methyl Orange. *Appl. Catal. B Environ.* **2003,** *42*, 187-201,

36. Ghazzal, M. N.; Wojcieszak, R.; Raj, G.; Gaigneaux, E. M., Study of Mesoporous CdS-Quantum-Dot-Sensitized TiO_2 Films by Using X-Ray Photoelectron Spectroscopy and AFM. *Beilstein J. Nanotechnol.* **2014,** *5*, 68-76,

37. Miller, D. J.; Biesinger, M. C.; McIntyre, N. S., Interactions of CO_2 and CO at Fractional Atmosphere Pressures with Iron and Iron Oxide Surfaces: One Possible Mechanism for Surface Contamination? *Surf. Interf. Anal.* **2002,** *33*, 299-305,

38. Su, C.; Liu, L.; Zhang, M.; Zhang, Y.; Shao, C., Fabrication of Ag/TiO_2 Nanoheterostructures with Visible Light Photocatalytic Function *via* a Solvothermal Approach. *CrystEngComm* **2012,** *14*, 3989-3999,

39. Zhang, H.; Liang, C.; Liu, J.; Tian, Z.; Wang, G.; Cai, W., Defect-Mediated Formation of Ag Cluster-Doped TiO_2 Nanoparticles for Efficient Photodegradation of Pentachlorophenol. *Langmuir* **2012,** *28*, 3938-3944,

40. *Handbook of X-Ray and Ultraviolet Photoelectron Spectroscopy*. Briggs, D., Ed. Heyden & Son LTD: Weinheim, 1979; Vol. 10, p 400

41. Boyen, H. G.; Kästle, G.; Weigl, F.; Koslowski, B.; Dietrich, C.; Ziemann, P.; Spatz, J. P.; Riethmüller, S.; Hartmann, C.; Möller, M.; Schmid, G.; Garnier, M. G.; Oelhafen, P., Oxidation-Resistant Gold-55 Clusters. *Science* **2002,** *297*, 1533,

42. Koslowski, B.; Boyen, H. G.; Wilderotter, C.; Kästle, G.; Ziemann, P.; Wahrenberg, R.; Oelhafen, P., Oxidation of Preferentially (111)-Oriented Au Films in an Oxygen Plasma Investigated by Scanning Tunneling Microscopy and Photoelectron Spectroscopy. *Surf. Sci.* **2001,** *475*, 1-10,

43. Wulff, G., On the Question of the Rate of Growth and Dissolution of Crystal Surfaces. *Z. Kristallogr. Mineral.* **1901,** *34*, 449-530,

44. Barnard, A. S.; Zapol, P.; Curtiss, L. A., Modeling the Morphology and Phase Stability of TiO_2 Nanocrystals in Water. *J. Chem. Theory Comput.* **2005,** *1*, 108-117,

45. Stankic, S.; Cortes-Huerto, R.; Crivat, N.; Demaille, D.; Goniakowski, J.; Jupille, J., Equilibrium Shapes of Supported Silver Clusters. *Nanoscale* **2013,** *5*, 2448-2453,

46. Majimel, J.; Lamirand-Majimel, M.; Moog, I.; Feral-Martin, C.; Tréguer-Delapierre, M., Size-Dependent Stability of Supported Gold Nanostructures onto Ceria: an HRTEM Study. *J. Phy. Chem. C* **2009,** *113*, 9275-9283,

47. Shahini, S.; Askari, M.; Sadrnezhaad, S. K., Gel–Sol Synthesis and Aging Effect on Highly Crystalline Anatase Nanopowder. *Bull. Mater. Sci.* **2011,** *34*, 1189-1195,

48. Ohtani, B.; Bowman, R. M.; Colombo, D. P., Jr.; Kominami, H.; Noguchi, H.; Uosaki, K., Femtosecond Diffuse Reflectance Spectroscopy of Aqueous Titanium(IV) Oxide Suspension: Correlation of Electron-Hole Recombination Kinetics with Photocatalytic Activity. *Chem. Lett.* **1998**, 579-580,

49. Dimitrijevic, N. M.; Shkrob, I. A.; Gosztola, D. J.; Rajh, T., Dynamics of Interfacial Charge Transfer to Formic Acid, Formaldehyde, and Methanol on the Surface of TiO_2 Nanoparticles and Its Role in Methane Production. *J. Phy. Chem. C* **2012,** *116*, 878-885,

50. Matthews, R. W., Kinetics of Photocatalytic Oxidation of Organic Solutes over Titanium Dioxide. *J. Catal.* **1988,** *111*, 264-272,

51. Mueller, R.; Kammler, H. K.; Wegner, K.; Pratsinis, S. E., OH Surface Density of SiO_2 and TiO_2 by Thermogravimetric Analysis. *Langmuir* **2003,** *19*, 160-165,

52. Mohamed, H. H.; Dillert, R.; Bahnemann, D. W., Growth and Reactivity of Silver Nanoparticles on the Surface of TiO_2: A Stopped-Flow Study. *J. Phy. Chem. C* **2011,** *115*, 12163-12172,

53. Kominami, H.; Murakami, S.-Y.; Kato, J.-I.; Kera, Y.; Ohtani, B., Correlation between Some Physical Properties of Titanium Dioxide Particles and Their Photocatalytic Activity for Some Probe Reactions in Aqueous Systems. *J. Phys. Chem. B* **2002,** *106*, 10501-10507,

54. Wojnicki, M.; Fitzner, K.; Luty-BŁOcho, M., Kinetic Studies of Gold Recovery From Dilute Aqueous Solutions Using Fe^{2+} Chloride Ions. *Trans. Nonferrous Met. Soc. China* **2015,** *25*, 2027-2036,

55. Mohamed, H. H. A. Kinetics and Mechanism of Charge Carrier Transfer Reactions at TiO_2 Nanoparticles Stopped-Flow and Laser Flash Photolysis Studies. PhD Thesis Gottfried Wilhelm Leibniz Universität, Hannover 2011.

56. Soejima, T.; Tada, H.; Kawahara, T.; Ito, S., Formation of Au Nanoclusters on TiO_2 Surfaces by a Two-Step Method Consisting of Au(III)-Complex Chemisorption and Its Photoreduction. *Langmuir* **2002,** *18*, 4191-4194,

57. Herrmann, J.-M., Photocatalysis Fundamentals Revisited to Avoid Several Misconceptions. *Appl. Catal. B Environ.* **2010,** *99*, 461-468,

58. Boxall, C.; Kelsall, G. H., Photoelectrophoresis of Colloidal Semiconductors Part 2.-Transient Experiments on TiO_2 Particles. *J. Chem. Soc., Farad. Trans.* **1991,** *87*, 3547-3556,

59. Tavassoli, Z.; Rodgers, G. J., Diffusive Growth of a Single Droplet with Three Different Boundary Conditions. *Eur. Phys. J. B - Cond. Matter and Complex Systems* **2000,** *14*, 139-144,

60. Curran, J. S.; Domenech, J.; Jaffrezic-Renault, N.; Philippe, R., Kinetics and Mechanism of Platinum Deposition by Photoelectrolysis in Illuminated Suspensions of Semiconducting Titanium Dioxide. *J. Phys. Chem.* **1985,** *89*, 957-963,

61. Bohren, C. F.; Huffman, D. R., *Absorption and Scattering of Light by Small Particles*. John Wiley and Sons: Weinheim 2007; p 530

62. Ghosh-Mazumdar, A. S.; Hart, E. J., Pulse Radiolysis Study of Bivalent and Zerovalent Gold in Aqueous Solutions. *Advan. Chem. Ser.* **1968,** *No. 81*, 193-209,

63. Harada, M.; Kizaki, S., Formation Mechanism of Gold Nanoparticles Synthesized by Photoreduction in Aqueous Ethanol Solutions of Polymers Using *in Situ* Quick Scanning X-Ray Absorption Fine Structure and Small-Angle X-Ray Scattering. *Cryst. Growth Des.* **2016,** *16*, 1200-1212,

64. Watzky, M. A.; Finke, R. G., Gold Nanoparticle Formation Kinetics and Mechanism: A Critical Analysis of the "Redox Crystallization" Mechanism. *ACS Omega* **2018,** *3*, 1555-1563,

65. Rodrigues, C. J.; Bobb, J. A.; John, M. G.; Fisenko, S. P.; El-Shall, M. S.; Tibbetts, K. M., Nucleation and Growth of Gold Nanoparticles Initiated by Nanosecond And Femtosecond Laser Irradiation of Aqueous $[AuCl_4]^-$. *Phys. Chem. Chem.Phys.* **2018,** *20*, 28465-28475,

66. Behar, D.; Rabani, J., Kinetics of Hydrogen Production upon Reduction of Aqueous TiO_2 Nanoparticles Catalyzed by Pd^0, Pt^0, or Au^0 Coatings and an Unusual Hydrogen Abstraction; Steady State and Pulse Radiolysis Study. *J. Phys. Chem. B* **2006,** *110*, 8750-8755,

67. Wojnicki, M.; Tokarski, T.; Kwolek, P., Kinetic Study of the Photoelectrochemical Gold Recovery from Diluted Chloride Solutions. *Arch. Metall. Mater.* **2013,** *58*, 709-716,

68. Chang, L.-H.; Yeh, Y.-L.; Chen, Y.-W., Preferential Oxidation of Co in Hydrogen Stream over Nano-Gold Catalysts Prepared by Photodeposition Method. *Int. J. Hydr. Ener.* **2008,** *33*, 1965-1974,

69. Sugimoto, T.; Zhou, X.; Muramatsu, A., Synthesis of Uniform Anatase TiO_2 Nanoparticles by Gel–Sol Method: 4. Shape Control. *J Coll. Interf. Sci.* **2003,** *259*, 53-61,

TOC: